

## Supporting Information

# Asynchronous-to-Synchronous Transition of Li Reactions in Solid-Solution Cathodes

*Nikhil Sharma,<sup>†</sup> Luize Scalco de Vasconcelos,<sup>†\*</sup> Shadad Hassan and Kejie Zhao\**

School of Mechanical Engineering, Purdue University, West Lafayette, IN 47907, USA

### Corresponding Authors

Kejie Zhao - [kjzhao@purdue.edu](mailto:kjzhao@purdue.edu)

Luize Scalco de Vasconcelos - [luizevasconcelos@utexas.edu](mailto:luizevasconcelos@utexas.edu)

## METHODS

### SAMPLE PREPARATION:

The NMC532 cathode used in the main experiment (Test 1 in Table S1) is prepared as follows. A slurry containing as-received  $\text{LiNi}_{0.5}\text{Mn}_{0.3}\text{Co}_{0.2}\text{O}_2$  powder (NMC532, Toda America), carbon black (CB, Denka), polyvinylidene fluoride (PVDF, Solvay, 5130), and n-methyl-2-pyrrolidone (NMP, Sigma Aldrich) is cast on a battery-grade aluminum sheet by slot-die coating. The areal loading was 12.5 mg per  $\text{cm}^2$ , and the weight ratios were 90 wt.% NMC532, 5 wt.% PVDF, and 5 wt.% CB. The calculated porosity of the cathode is 55%. A strip of 0.8  $\text{cm}^2$  area was cut out of the cathode and ion polished (JEOL IB-19500CP, rotating stage) to achieve a flat and smooth surface suitable for high magnification optical imaging. The scanning electron microscopy (SEM) images in Figure S8 show the surface morphology pre- and post-polishing.

### OPERANDO SETUP AND EXPERIMENTS:

The cathode sample was then kept overnight in a vacuum oven at 80°C to remove moisture. Next, the sample was transferred to an argon-filled glovebox ( $O_2$  and  $H_2O < 1$  ppm) and fixed to the center of a fluid cell to serve as the working electrode (W.E.) and wrapped around by a non-contacting Li metal ribbon (99.9% Li, Sigma Aldrich) which served as the counter electrode (C.E.). The cell is filled with a non-volatile electrolyte consisting of 0.75M of  $LiPF_6$  in propylene carbonate (PC, Sigma Aldrich) and ethylene carbonate (EC) with a 1:1 weight ratio. The cell is cycled using a potentiostat (VersaSTAT 4, Princeton Applied Research, Ametek) and optical images (integrated microscope, Keysight G200 nanoindenter) acquired every minute at fixed positions. At the cut-off voltages (high 4.3V and low 2.5V), we maintain a constant potential until the current drops to 1/5 of the galvanostatic current to achieve a better coulombic efficiency. Tests are conducted at C/20 and C/10 (1C = 200 mA/g). 100% SOC is defined as the capacity at the end of the first charging of the pristine sample after the voltage hold. In addition to the main experiment, we conduct additional tests to verify the generality of the findings for different test conditions (Tests 2 and 3 in Table S1). To test a more commonly used but volatile diethyl carbonate (DEC) based electrolyte (Test 3 in Table S1), we design a sealed fluid cell (Figure S9) that can be tested outside the glovebox without air contamination (Figure S10). Test 2 in Table S1 verifies that the experimental observations are also repeatable for different transition metal ratios ( $LiNi_{0.8}Mn_{0.1}Co_{0.1}O_2$ , NMC811, MTI Corp.),

types of binder (Polyacrylic acid, PAA, Sigma Aldrich), and polishing procedures. For ion polishing, we use the JEOL IB-19500CP with rotating stage. For mechanical polishing, we use the Buehler Ecomet 3000 with 0.05  $\mu\text{m}$  silica slurry on imperial cloth by LECO Co.



## Supporting Note S1

Theoretical modeling: The Butler-Vomer equation represents the charge transfer kinetics occurring at the interface between the active material NMC and the electrolyte. CB partially covers the surface of the NMC particles, and the rest of the NMC surface is exposed to the electrolyte. Li-ions transporting through the electrolyte meet the electrons traveling from the cathode current collector through the CB domain on the surface of the NMC particles. Because of the inhomogeneous coverage of the NMC particle surface by the CB, we consider electron transport in NMC through a thin shell with a thickness of  $s$  on the surface. The electric potential ( $\phi_S$ ) variation in the thin shell has a relationship with the surface current ( $i_{surf}$ ) and the current from the CB domain ( $i_S$ ) as follows:

$$i_{surf} = -K_{NMC} \nabla_{surf} \phi_S,$$

$$\nabla_{surf} \cdot (s i_{surf}) = i_S.$$

The boundary conditions of charge transfer at the electrolyte & NMC interface are:

$$i_l \cdot \mathbf{n} = -i_{BV}, \quad i_S \cdot \mathbf{n} = i_{BV}.$$

The boundary conditions for the mass conservation at the electrolyte & NMC interface give:

$$J_l \cdot \mathbf{n} = -\frac{i_{BV}}{F}, \quad J_{NMC} \cdot \mathbf{n} = \frac{i_{BV}}{F}.$$

where  $\mathbf{n}$  is the normal unit vector at the specified surfaces.

For the homogenized carbon binder domain, porosity is defined as  $\epsilon_l$  and the carbon binder fraction is defined as  $\epsilon_{CB}$ ,  $\epsilon_l + \epsilon_{CB} = 1$ . Hence using the Bruggeman relationship, the effective bulk transport equations for the electrolyte within the porous carbon binder domain are:

$$D_{l\_eff} = \epsilon_l^{1.5} \cdot D_l$$

$$K_{l\_eff} = \epsilon_l^{1.5} \cdot K_l$$

$$K_{CB\_eff} = \epsilon_l^{1.5} \cdot K_{CB}$$

It is worth noting that the reaction rate constant's ( $k$ ) contribution towards the charge heterogeneity is minimal in our model, as indicated by the comparison of the composition spatiodynamics using concentration-dependent  $k$  values versus the constant  $k$  value shown in Figure S7.

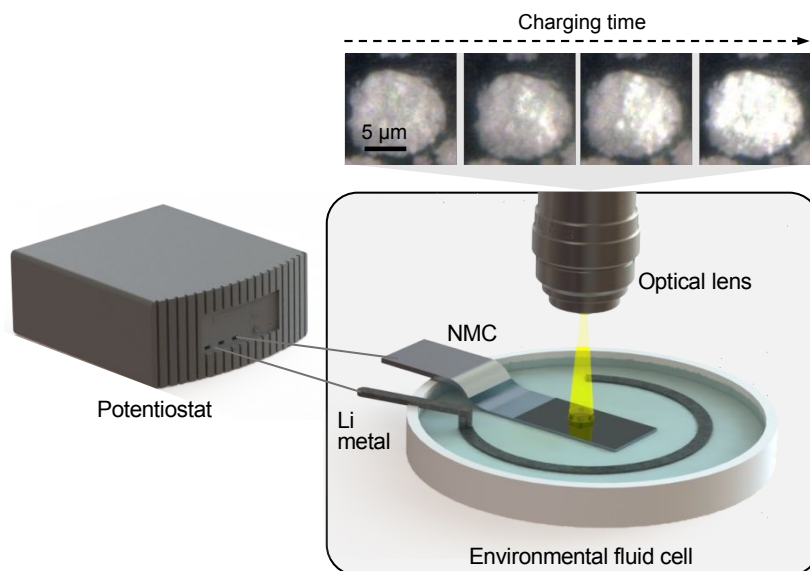


**Figure S1.** Experimental setup for operando optical imaging of battery electrodes while undergoing controlled electrochemical cycling in an inert gas environment. The fluid cell contains a surface polished NMC cathode (W.E.) enclosed by a Li metal ribbon (C.E.) inside an electrolyte container that connects to a potentiostat. The continuous imaging of the cathode's top surface shows that the optical reflectivity of the NMC particle changes with the Li content in the cathode.

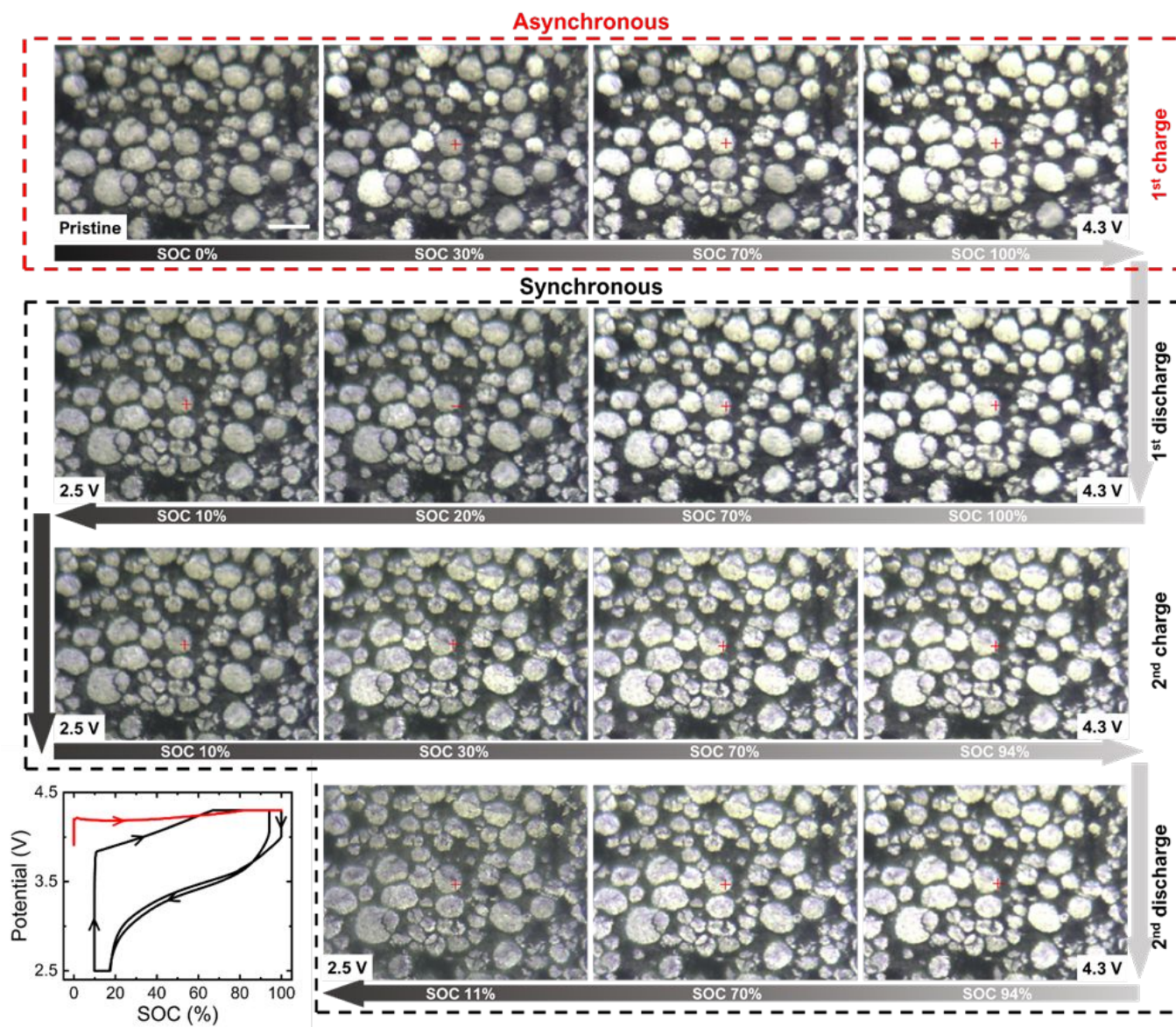


**Figure S2.** Potential curve and corresponding optical images of an NMC532 cathode during its first two cycles at  $C/20$ . The reflectivity of the NMC particles changes with the SOC leading to the varying pixel intensity. During the 1<sup>st</sup> charge (first row), particle intensities change asynchronously and abruptly from dark to bright (white scale bar 20  $\mu\text{m}$ ). Distinctively, subsequent (dis)charge processes proceed through a gradual and synchronous change in reflectivity. The high reflective intensity corresponds to the delithiated state (end-of-charge, 4.3V), and the low intensity corresponds to the lithiated state (end-of-discharge, 2.5V).

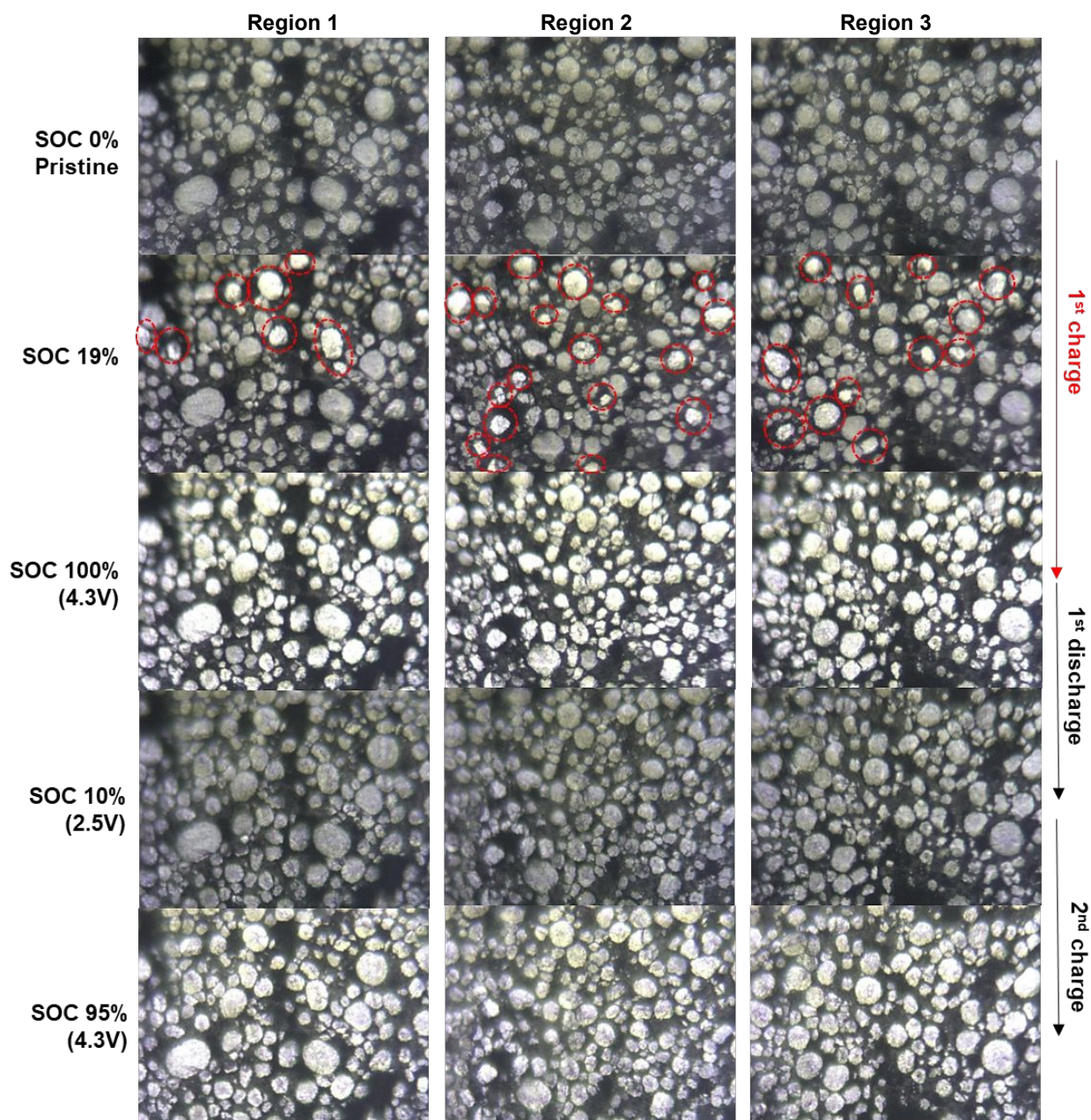


**Figure S3.** Evidence of asynchronous charging of the NMC532 particles in multiple regions across the electrode. The red circles highlight the particles that underwent a sudden change of the optical reflection during the initial 19% charging.

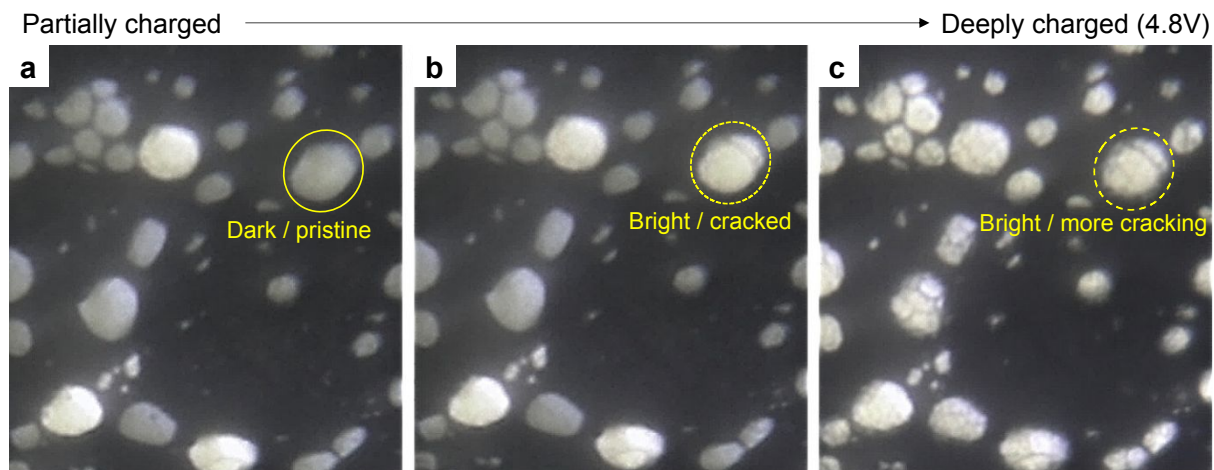


**Figure S4.** Observation of the asynchronous 1<sup>st</sup> charging and particle cracking of NMC811 (Test 2 in Table S1). At timestep (a) there are three bright particles (reacted) while the rest remains dark (unreacted). From timestep (a) to (b) the circled particle lights up (reacts), and at the same time, a large crack appears. At the end of deep delithiation (c), there is extensive cracking throughout the cathode. The white scale bar is 10  $\mu\text{m}$ .

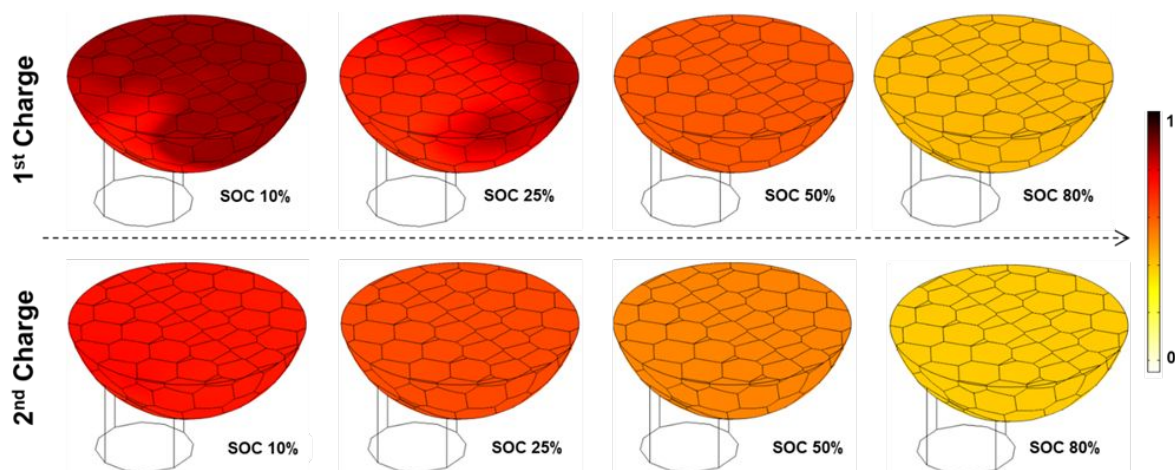


**Figure S5.** 3D model of a single surface polished NMC secondary particle in contact with a carbon binder (black outlines) and submerged in the electrolyte. The intraparticle heterogeneity in the first charging process and subsequent homogeneous Li distribution agrees with the experimental observation (Figure 2 and Figure 3). This transition in the compositional spatiodynamics results from the incomplete Li intercalation in NMC after the first cycle.

## Supporting Note S2

The diffusion anisotropy in the secondary particles contributes to the intra-particle concentration heterogeneity. This effect is apparent as the initial spread of the normalized surface concentration plots during the initial stage of the 1<sup>st</sup> charge in Figure 4d (each color represents a particle and different lines of the same color correspond to concentration profile at different positions on that particle's surface). We also performed modeling for a single 3D particle with a small carbon binder region attached to its curved surface and surrounded by the electrolyte to understand the intraparticle heterogeneity, as shown in Figure S5. For the 3D model, the diffusional anisotropy, together with the specific location where the carbon binder contacts with the NMC particle, can influence the front propagation direction. In agreement with the experimental observation, this behavior is shown only during the 1<sup>st</sup> charge but not in subsequent (dis)charge cycles. The local electric potential of the NMC particle ( $\phi_s$ ) will heavily control the time at which the front initiates during the 1<sup>st</sup> charge. This, in turn, largely depends on how the electrical conduction barriers (in the form of NMC particle surfaces) are embedded along the electrically conductive path from the current collector. We also observe the same behavior of front propagation in experiments using a different electrolyte paired with the NMC532 cathode (Supporting Figure S6).

For the 2D model, we assign preferential diffusivity along the randomly aligned axis of the primary particles and assume the planer diffusivity as 1/100 of the preferential diffusivity value along the perpendicular direction.

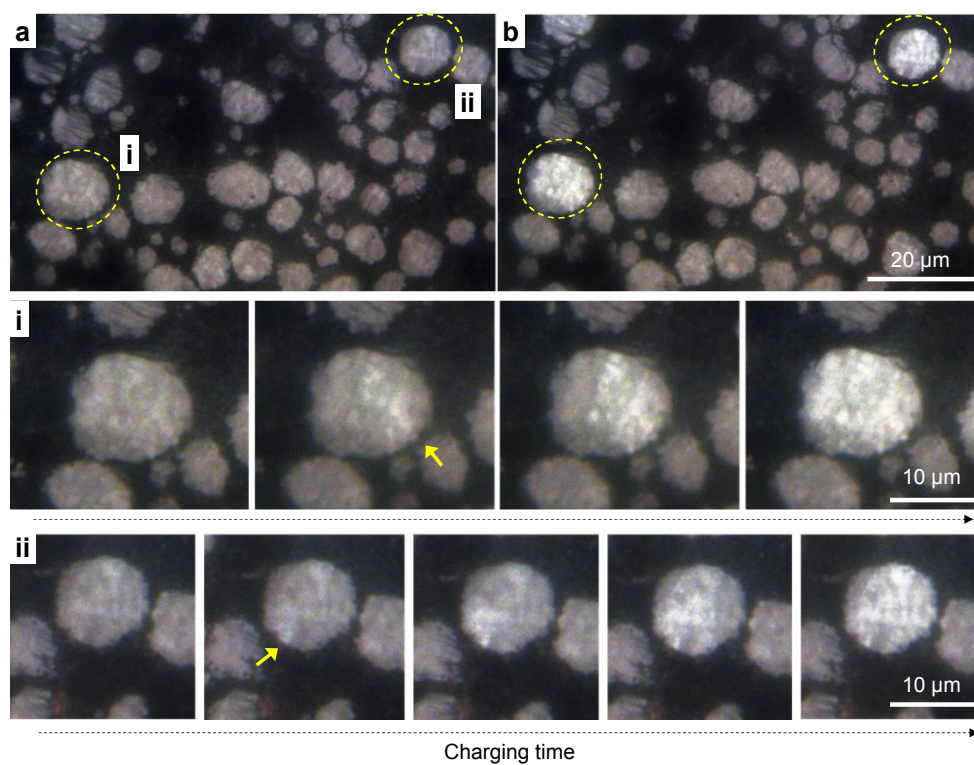


**Figure S6.** Optical images of the first charging of NMC532 in 1M LiPF<sub>6</sub> in EC:DEC electrolyte using the sealed fluid cell (Test 3 in Table S1). (a) Pristine and (b) partially charged samples show a propagating reaction front observed in two NMC particles while the remaining particles experience no intensity change. The original brightness setting for the experiment was not optimum for this microscope lens (100X), and the overall picture brightness and contrast were post-processed for clarity in this figure. The movie with original raw image capture settings without post-processing is included in Video S2 for reference.

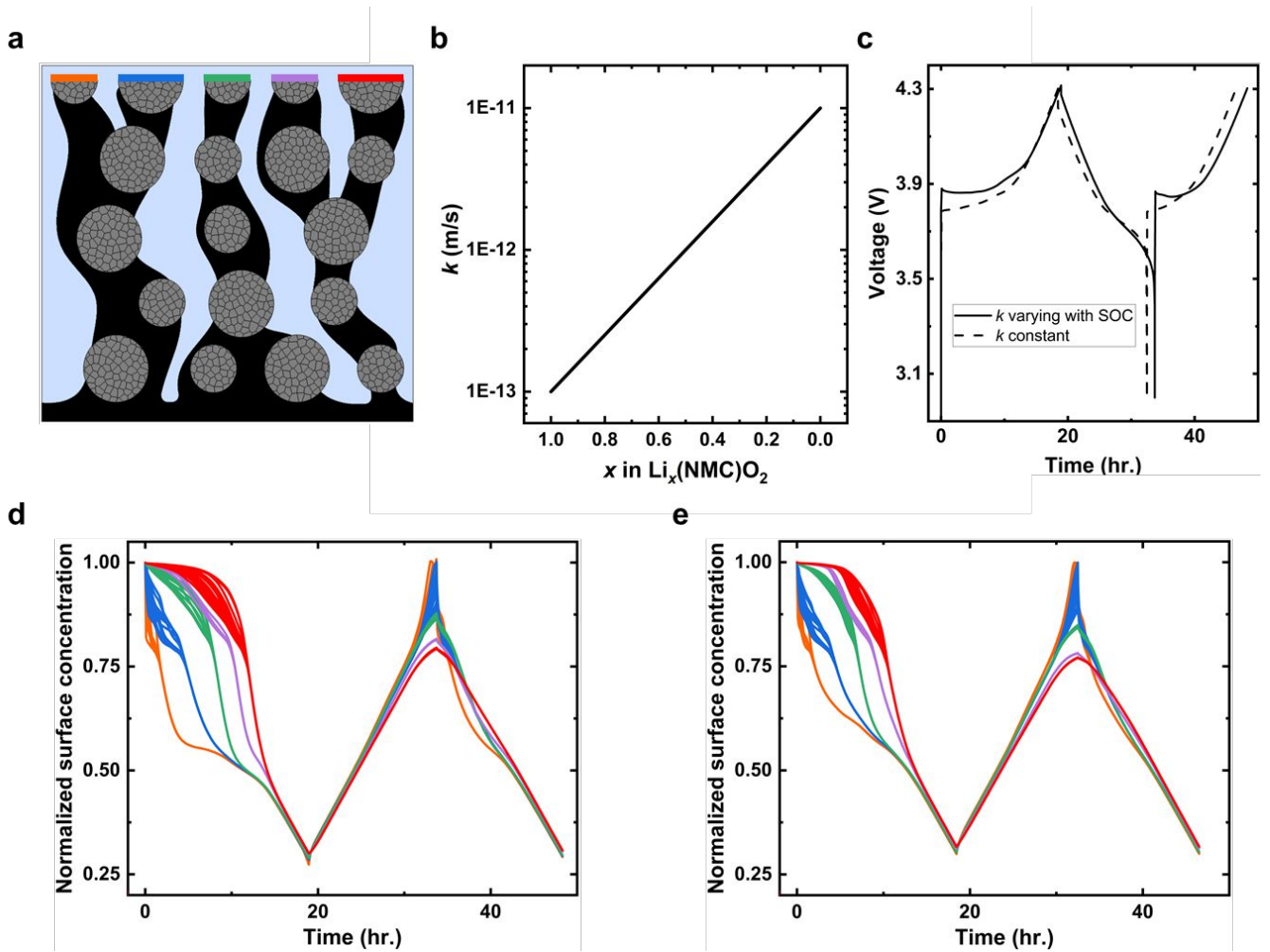


**Figure S7.** Li concentration profiles at the surface of the topmost particles as a function of time during the charge-discharge-charge process. (a) Different colors represent different particle surfaces with dissimilar electrical connections. (b) Reaction rate varying with SOC. (c) Voltage curves as a function of time for (d) in the solid line and (e) in the dotted line. The voltage represents the difference in electric potential at the bottom surface (cathode current collector) and the top surface (Li metal surface). (d) Concentration profiles for the reaction rate constant ( $k$ ) varying with the SOC. (e) Concentration profiles for the reaction rate constant  $k = 1 \times 10^{-12}$  m/s.

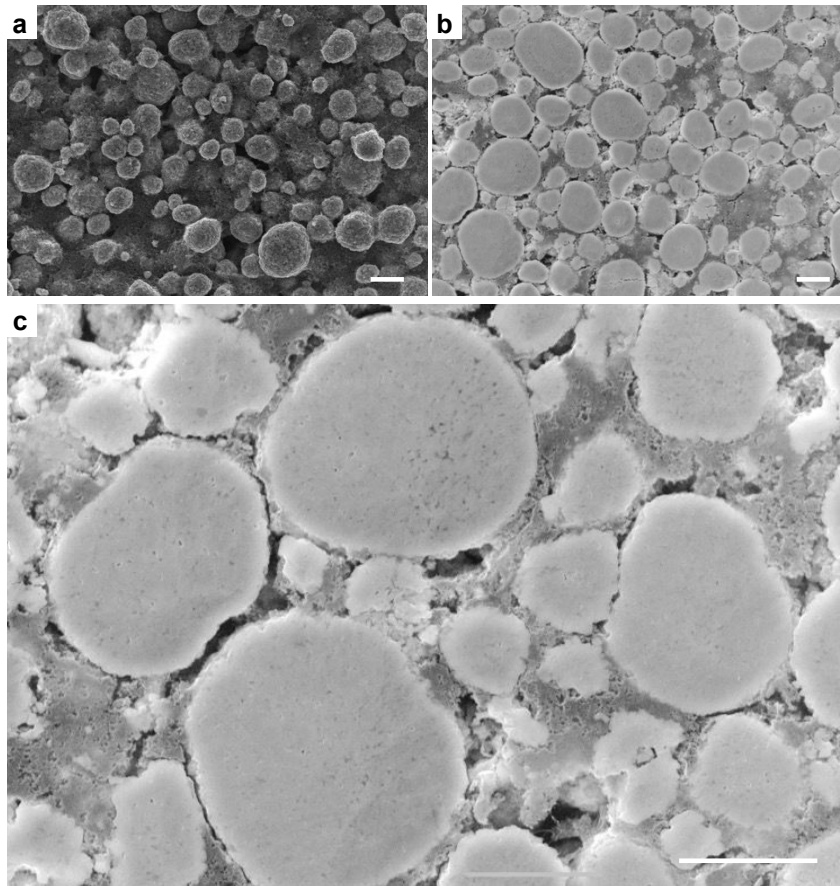


**Figure S8.** Scanning electron microscopy (SEM) images of the NMC cathode (a) before and (b), (c) after surface polishing. Scale bars correspond to 10  $\mu\text{m}$ .

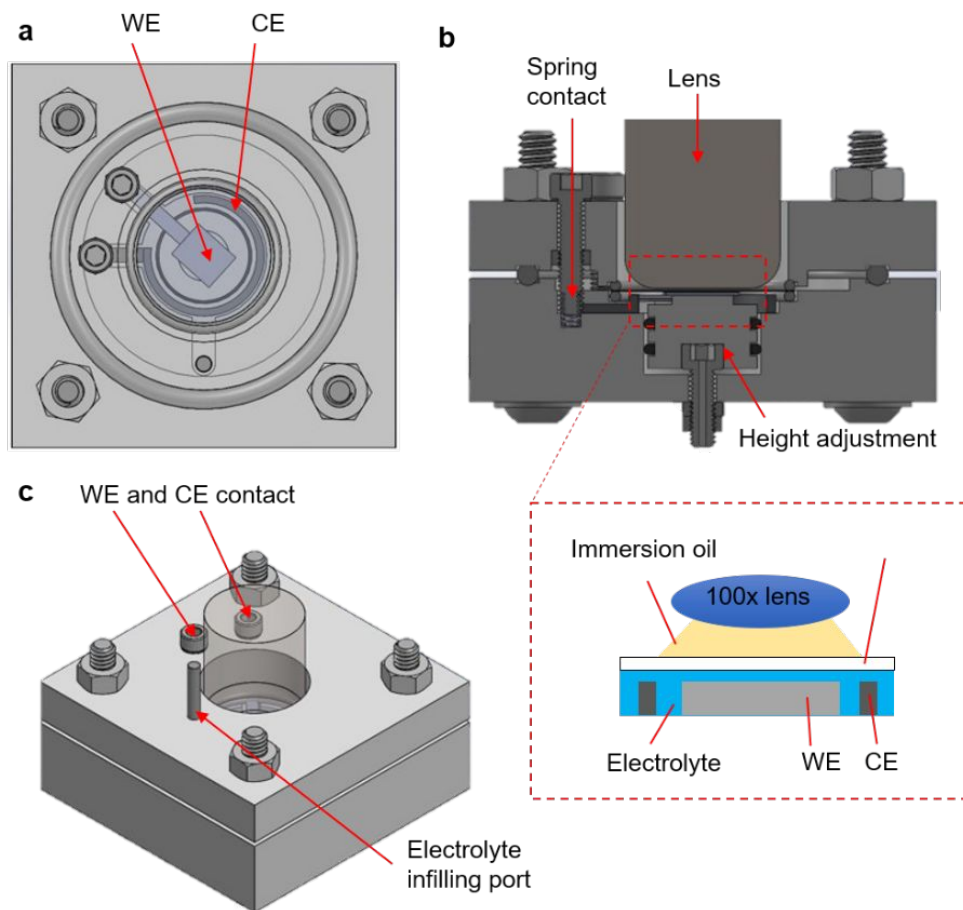


**Figure S9.** Setup of a closed cell for in-situ optical experiments. The cathode (W.E.) is kept on a movable platform, with the anode (C.E.) lying on the circumferential groove in the electrolyte-filled chamber.

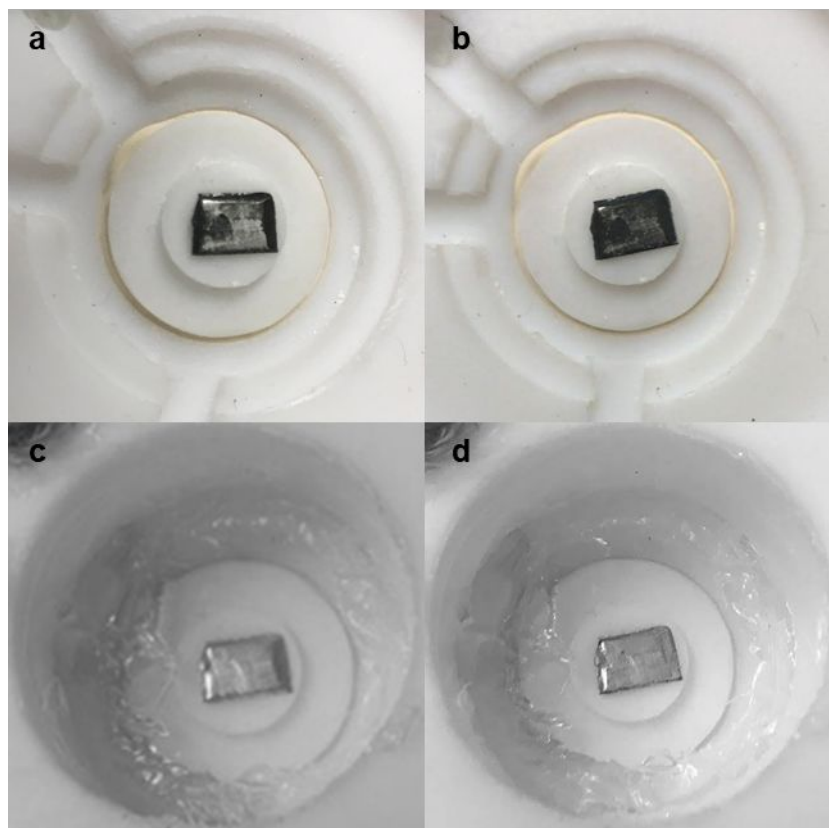


**Figure S10.** Leakage test of the sealed fluid cell using a Li metal. Li metal quickly oxidizes after (a) 9 mins and (b) 16 mins of air exposure. Li metal inside the sealed cell after (c) 16 hours and (d) 3 days outside the glovebox maintains its shininess.

**Table S1.** Supplementary tests performed to verify the generality of the discovered asynchronous 1<sup>st</sup> charging effect.

Test	Composition	Preparation	Electrolyte	Environment	C-rate
1	NMC532/PVDF/CB	Ion polish	0.75M LiPF <sub>6</sub> in PC:EC	Glovebox	C/20
2	NMC811/PAA/CB	Manual polish	0.75M LiPF <sub>6</sub> in PC:EC	Glovebox	C/20
3	NMC532/PVDF/CB	Ion polish	1M LiPF <sub>6</sub> in EC:DEC	Sealed cell	C/10

**Table S2.** Equations for the homogenized CB domain.

---

Electrolyte current density	$\mathbf{i}_l = -K_{l,eff}\nabla\phi_l + \frac{2K_{l,eff}RT}{F}\left(1 + \frac{\partial \ln f}{\partial \ln c_l}\right)(1 - t_+)\nabla \ln c_l$
Current density	$\mathbf{i}_s = -K_{CB,eff}\nabla\phi_{CB}$
Charge conservation	$\nabla \cdot \mathbf{i}_l = 0 \quad \nabla \cdot \mathbf{i}_s = 0$
Li flux	$\mathbf{J}_l = -D_{l,eff}\nabla c_l + \frac{\mathbf{i}_l t_+}{F}$
Mass conservation	$\frac{\partial c_l}{\partial t} + \nabla \cdot \mathbf{J}_l = 0$

---

**Table S3.** Equations for the electrolyte & NMC particles.

	Electrolyte	NMC
Electrolyte current density	$\mathbf{i}_l = -K_l \nabla \phi_l + \frac{2K_l RT}{F} \left(1 + \frac{\partial \ln f}{\partial \ln c_l}\right) (1 - t_+) \nabla \ln c_l$	-
Charge conservation	$\nabla \cdot \mathbf{i}_l = 0$	-
Li flux	$\mathbf{J}_l = -D_l \nabla c_l + \frac{\mathbf{i}_l t_+}{F}$	$\mathbf{J}_{NMC} = -D_{NMC} \nabla c_{NMC}$
Mass conservation	$\frac{\partial c_l}{\partial t} + \nabla \cdot \mathbf{J}_l = 0$	$\frac{\partial c_{NMC}}{\partial t} + \nabla \cdot \mathbf{J}_{NMC} = 0$

**Table S4.** Numerical values of the parameters in the modeling.

Parameter Name	Symbol (unit)	Value
Universal gas constant	$R$ ( $\text{J} \cdot \text{mol}^{-1} \cdot \text{K}^{-1}$ )	8.314
Temperature	$T$ (K)	298
Faraday's constant	$F$ ( $\text{A} \cdot \text{s} \cdot \text{mol}^{-1}$ )	96485
Transference number	$t_+$	0.363
Anodic transfer coefficient	$\alpha_a$	0.5
Cathodic transfer coefficient	$\alpha_c$	0.5
Molar activity of electrolyte	$f$	0.43
Anodic & cathodic reaction rate coefficient	$k$ (m/s)	1e-11
Electrical conductivity of CB	$K_{\text{CB}}$ (S/m)	1000
Electrical conductivity of NMC	$K_{\text{NMC}}$ (S/m)	Fig. 4b
SOC range (max. – min.)	–	0.97 – 0.3
Diameter of NMC secondary particles	$d$ ( $\mu\text{m}$ )	10 & 14
Maximum concentration of Li in NMC	$C_{\text{max.}}$ ( $\text{mol}/\text{m}^3$ )	49000
Initial concentration of Li in NMC	$C_{\text{ini}}$ ( $\text{mol}/\text{m}^3$ )	47530
Reference electrolyte concentration	$C_{l,\text{ref}}$ ( $\text{mol}/\text{m}^3$ )	1
Li diffusivity in NMC	$D$ ( $\text{m}^2/\text{s}$ )	Fig. 4c

Electrochemical equilibrium potential of NMC	$E_{eq}(V)$	Supporting Ref. 1
Shell thickness on NMC surface	$s$ (nm)	10

---

**Supporting Video Captions:**

**Video S1.** Optical microscopy video of NMC532 during the first two (dis)charge cycles at C/20 demonstrating asynchronous charging behavior during the 1st charge only. CC represents constant current (dis)charging. CV represents constant voltage (dis)charging.

**Video S2.** 1st charge optical microscopy video of NMC532 in 1M LiPF<sub>6</sub> in EC:DEC electrolyte at 100X optical microscope lens (Test 3 in Table S1).

## Supporting References

1. Weber, R.; Fell, C. R.; Dahn, J. R.; Hy, S. Operando X-Ray Diffraction Study of Polycrystalline and Single-Crystal  $\text{Li}_x\text{Ni}_{0.5}\text{Mn}_{0.3}\text{Co}_{0.2}\text{O}_2$ . *J. Electrochem. Soc.* **2017**, *164* (13), A2992–A2999.

<https://doi.org/10.1149/2.0441713jes>.